Multiattribute seismic analysis on AVO-derived parameters—A case study

SATINDER CHOPRA, Core Lab Reservoir Technologies, Calgary, Canada
DOUG PRUDEN, GEDCO, Calgary, Canada

Prospecting for reservoir zones in mature trends sometimes requires unconventional exploration tools. AVO has been successfully used as a direct hydrocarbon indicator in some clastic rocks. Lately, AVO inversion for Lamé parameters ($\lambda\rho$ and $\mu\rho$) has been shown to enhance identification of reservoir zones. Furthermore, integration of AVO-derived attribute volumes with other non-AVO-derived seismic attribute volumes can provide meaningful geologic information when tied back to well data and verified as correlating with rock properties. This paper provides a case study of a 3D seismic survey in southern Alberta, Canada, where a probabilistic neural network solution was employed on AVO attributes. The results were integrated with other seismic attributes to develop a more comprehensive interpretation.

The target area is a Lower Cretaceous glauconite-filled (cycles of shales and quartz sandstones) fluvial channel, deposited within an incised valley system. A 3D seismic survey was acquired to create a stratigraphic model consistent with all available well control and matching the production history. The ultimate goal was to locate undeveloped potential within the gas sands. The field has been producing since the early 1980s and two of the earliest, most prolific producers have begun to water out.

As the objective was stratigraphic in nature, the seismic data were processed with the objective of preserving relative amplitude relationships in the offset domain to allow for AVO attribute analysis.

Time slice animation of the processed 3D migrated volume indicated the presence of a main valley cut in the northeast corner of the survey. A Coherence Cube analysis of the 3D survey enhanced the channel features that were evident on the well data. The data were datumed on an easily mapped Upper Cretaceous marker to remove the distortions of regional dip from time slices at the zone of interest. Figure 1a shows a horizon slice through the coherence volume at the reservoir level.

The complex trace envelope attribute is generally used for mapping lithology changes. A composite volume containing the envelope attribute superimposed on the coherence data is shown in Figure 1b. High envelope values are seen within the incised valley; however, they do not provide information that separates tight lithic sands from productive glauconite sands.

Because this reservoir has been depleted by gas production, high amplitude anomalies are not necessarily indicative of significant gas accumulations. Only a minor presence of gas is required within pore spaces to produce significant seismic amplitude effects. It has been reported (Diaz et al., 2001) that glauconitic sandstone reservoir rocks can be delineated using Poisson's ratio and AVO acoustic impedance inversion analysis. The generation and calibration of synthetic seismograms with full-offset-stacked migrated 3D data resulted in mis-ties, suggesting the possibility of AVO effects due to lithology and pore fluid fill. The near-trace stack approximates a more normal incidence model, as assumed in the synthetic seismograms, and improves the well ties. From this analysis, it was determined that AVO inversion for Lamé rock parameters could provide additional insight into the geologic complexity.

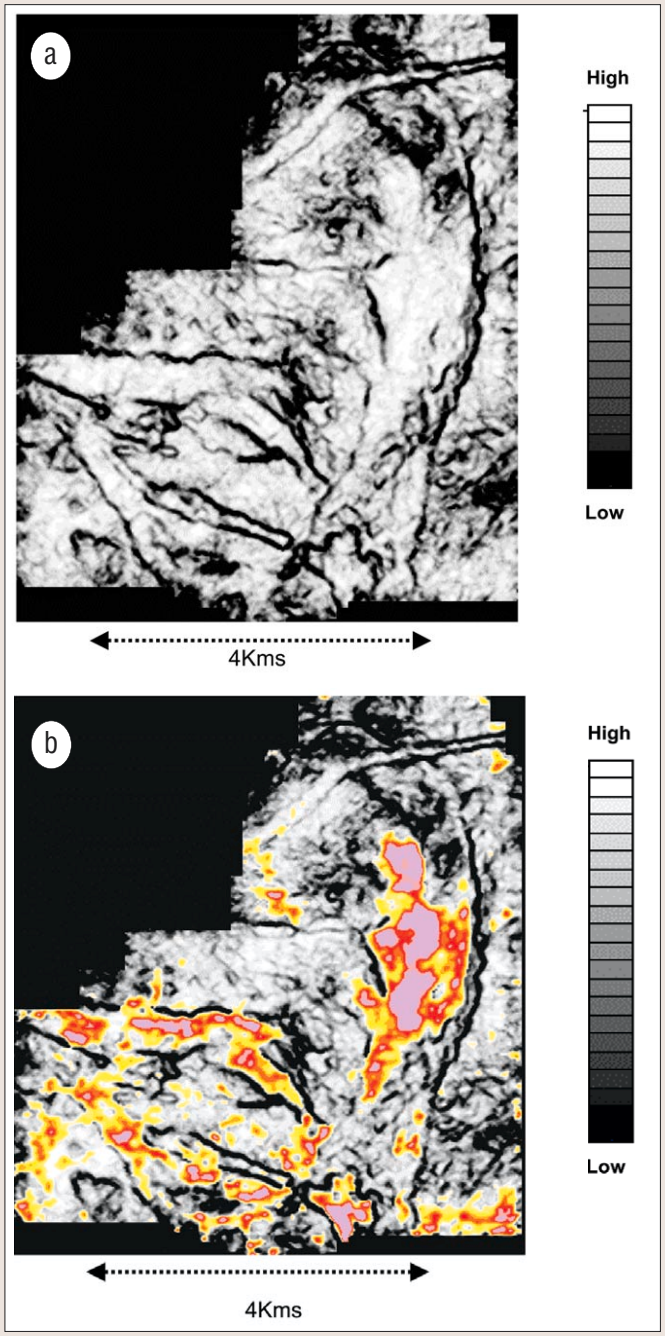

Figure 1. (a) Horizon slice through the coherence volume at the level of the reservoir. The definition of the main incised valley now seems quite clear. (b) A composite volume containing the complex trace envelope attribute (in color) as well as the coherence coefficients. High envelope amplitudes are seen within the incised valley. However, although these displays are quite revealing, they do not provide information that can separate tight lithic sands from productive glauconite sands.

AVO inversion for Lamé rock parameters. Reservoir properties can be defined in terms of fundamental rock para-

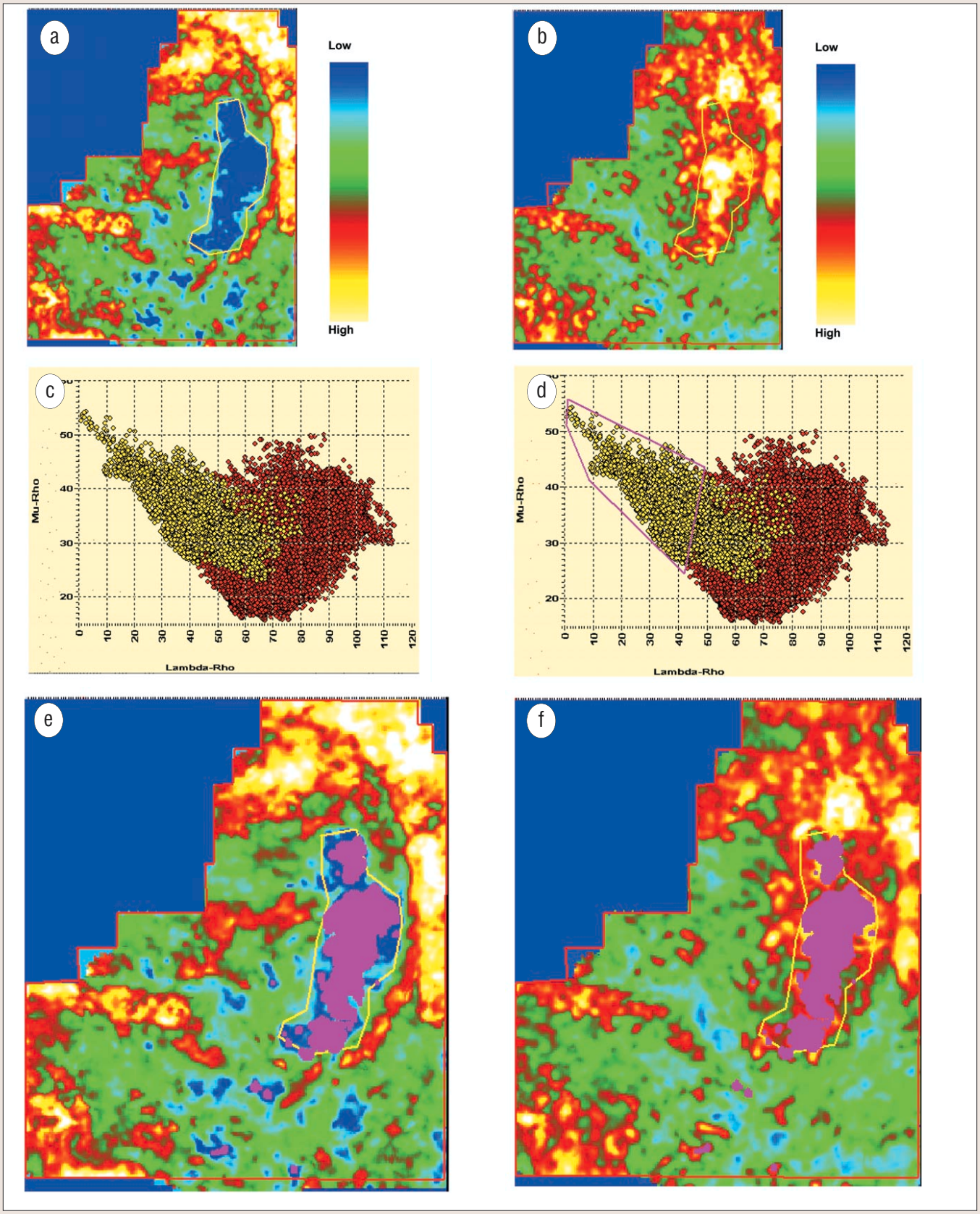

Figure 2. *(a) Horizon slice from Lambda-Rho volume showing the suspected gas anomaly. Low values of Lambda-Rho are blue. (b) Horizon slice from Mu-Rho volume showing the suspected gas anomaly. High values of Mu-Rho are yellow and red. (c) Lambda-Rho plotted against Mu-Rho. The yellow points come from the yellow polygon which encloses the suspected anomaly in Figures 2a and 2b. The red points come from the red polygon that encloses all live data points on the horizon slices. The plot shows that the yellow points correspond to low values of Lambda-Rho and high values of Mu-Rho (as expected of a gas anomaly). (d) The points within the purple polygon represent low values of Lambda-Rho and high values of Mu-Rho. These points are highlighted on Figures 2e and 2f, confirming the anomaly. (e) Horizon slice from Lambda-Rho volume highlighting the portions corresponding to low values of Lambda-Rho and high values of Mu-Rho (purple polygon in Figure 2d). (f) Horizon slice from Mu-Rho volume highlighting the portions corresponding to low values of Lambda-Rho and high values of Mu-Rho (purple polygon in Figure 2d).*

meters such as incompressibility and rigidity. Goodway et al. (1997) suggested the use of Lambda-Mu-Rho analysis to extract lithology and pore fluid information from seismic and well log data. The basic theory for this analysis has been discussed by Burianyk (2000), Goodway (2001), Ma (2001), and Dufour et al. (2002).

P-wave and S-wave impedance reflectivity responses were estimated by solving the Fatti simplification of the Zoeppritz equations:

$$R = \frac{1}{2}(1+\tan^2\theta)\frac{\Delta I_p}{I_p} - 4\left(\frac{V_s}{V_p}\right)^2 \sin^2\theta\,\frac{\Delta I_s}{I_s}$$

where $\frac{\Delta I_p}{I_p}$ = P-wave impedance reflectivity

$\frac{\Delta I_s}{I_s}$ = S-wave impedance reflectivity

The V_P/V_S ratio was estimated from dipole sonic log data proximal to the area of study.

Impedance reflectivities are related to Lamé parameters of incompressibility (λ) and rigidity (μ) by the relationships $\lambda\rho = I_p^2 - 2I_s^2$ and $\mu\rho = I_s^2$ where ρ is bulk density.

The Lamé parameters cannot be directly extracted without an estimation of the density parameter ρ.

Inversion for geologic parameters. AVO inversion as described above yields several seismic attribute volumes which all contain fluid and lithological information. These volumes are: density scaled compressibility, density scaled rigidity, derived normal incidence P-wave stack, P impedance reflectivity, S impedance reflectivity, and fluid factor stack.

Figures 2a and 2b show the Lambda-Rho and Mu-Rho sections with an anomaly enclosed in a yellow polygon. The plots for these two attributes are also shown in Figures 2c and 2d. The yellow dots represent the values within the polygons on Figures 2a and 2b, respectively. The red polygon in Figure 2d indicates where we would expect to find gas sands in Lambda-Rho and Mu-Rho space. In addition to gas-sand identification, significant lithological information can be derived from the data.

Multivariate statistical analysis can be used as an aid in determining whether the derived property volumes are related to gas saturation and lithology. Our approach examines the relationship between variables to determine whether common clusters or groupings will form that represent a particular lithology or fluid fill. Figures 2c and 2d show a two-dimensional example of this approach in which gas sands tend to separate themselves in Lambda-Rho, Mu-Rho space (pink polygon in Figure 2d). This approach becomes less intuitive when more than three variables are considered simultaneously. It is difficult to visualize n-dimensional cross-plot space if n is greater than four even when color is used as a fourth dimensional separator. It is within this n > 4 space that clustering or separation of differing lithology and fluid fill may be most evident.

Figure 3 is an example of the separation power of cluster analysis. Within the zone of interest, the value for each of the six variables has been subjected to a k-means cluster separation analysis, assuming that four distinct classes exist within the data set. As can be seen in Figure 3, the cluster separation has divided the data into separate zones, based on the common relationships between the variables.

This type of unsupervised cluster separation analysis is often capable of creating useful character mappings of the data in 3D space by reducing a large number of attributes down to one (assigned cluster) that can be visualized on a map. Figure 4 is a small subset of the larger 3D that has had this analysis performed. Different clusters may tend to associate themselves with differing lithologies which can be verified by well data.

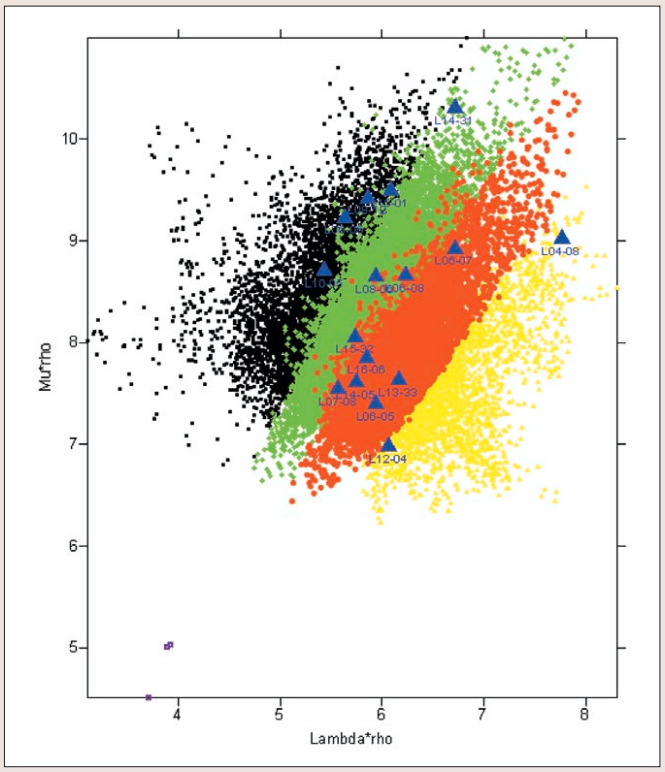

Figure 3. *Lambda-Rho plotted against Mu-Rho with multiattribute cluster classifications and posted values at wells within the study area.*

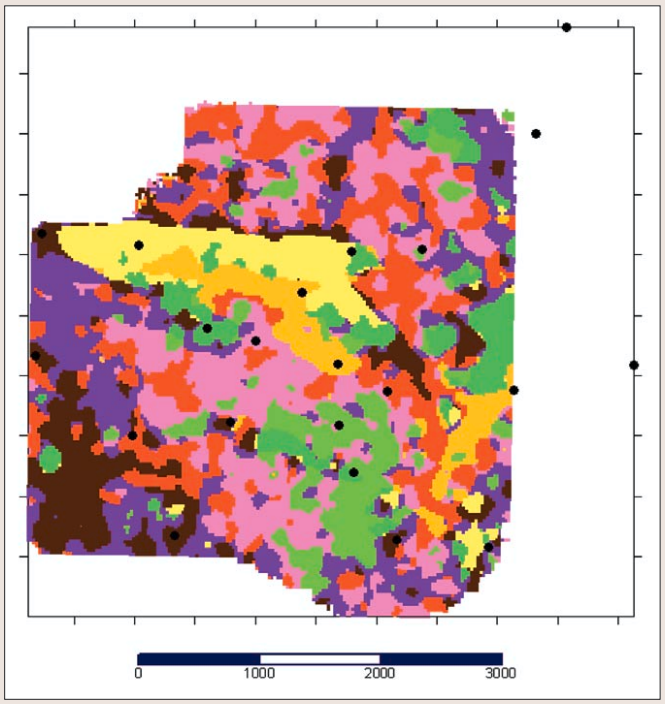

Figure 4. *A subset of the 3D volume of the study area that has been subjected to K-means cluster analysis. Note that the analysis appears to reveal some lithological information, but the clusters have not yet been subjected to classification according to the well control.*

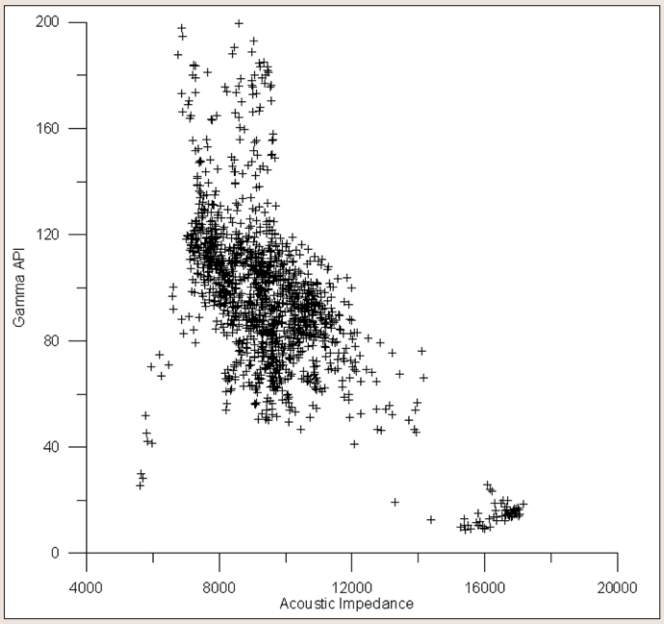

Figure 5. *API gamma-ray values plotted against acoustic impedance. Note the nonlinear nature of the relationship.*

Analysis of this type has many inherent limitations. (1) The results are sensitive to the number of clusters selected by the user. Testing is necessary in order to avoid underestimating or overestimating the number of clusters that adequately represent the data. (2) There is no guarantee that the derived clusters have anything to do with the lithology or fluid fill. The results must be calibrated to the well control. (3) There is no guarantee that the wells have exhaustively sampled the geologic space, or that the existing well control is representative of the statistical variability of the lithology.

In this area, gamma ray logs are diagnostic of sands and exist for each well. There is also a fairly even sampling of well data across the field. Therefore a deterministic approach was found that allowed us to quantitatively relate the measured seismic attributes to the gamma ray data. A simple analysis of the relationship of gamma ray values to acoustic impedance (Figure 5) suggests that, while a general relationship between the two is visually apparent, it is clearly a nonlinear relationship. Further analysis of the other attributes with the gamma ray curve produces similar results.

A nonlinear multivariate determinant analysis between the derived multiple seismic attribute volumes and the measured gamma ray values at wells is a problem ideally suited for neural networks. By training a neural network with a statistically representative population of the targeted log responses and the multiple seismic attribute volumes available at each well, a nonlinear multiattribute transform can be computed to produce an inversion volume of the targeted log type.

Using the gamma ray, acoustic, and bulk density log curves available over the zone of interest for the 16 wells, the procedure described by both Hampson et al. (2001) and Leiphart and Hart (2001) was employed to derive gamma ray and bulk density inversions across the 3D volume.

Discussion of results. The resulting gamma ray inversion is shown on the horizon slice in Figures 6a and 6b (the same slice shown previously). The data are scaled to API gamma units in Figure 6a and converted to porosity in Figure 6b using the following standard linear density relationship (Schlumberger, 1989):

$$\rho_b = \phi\rho_f + (1-\phi)\,\rho_{ma}$$

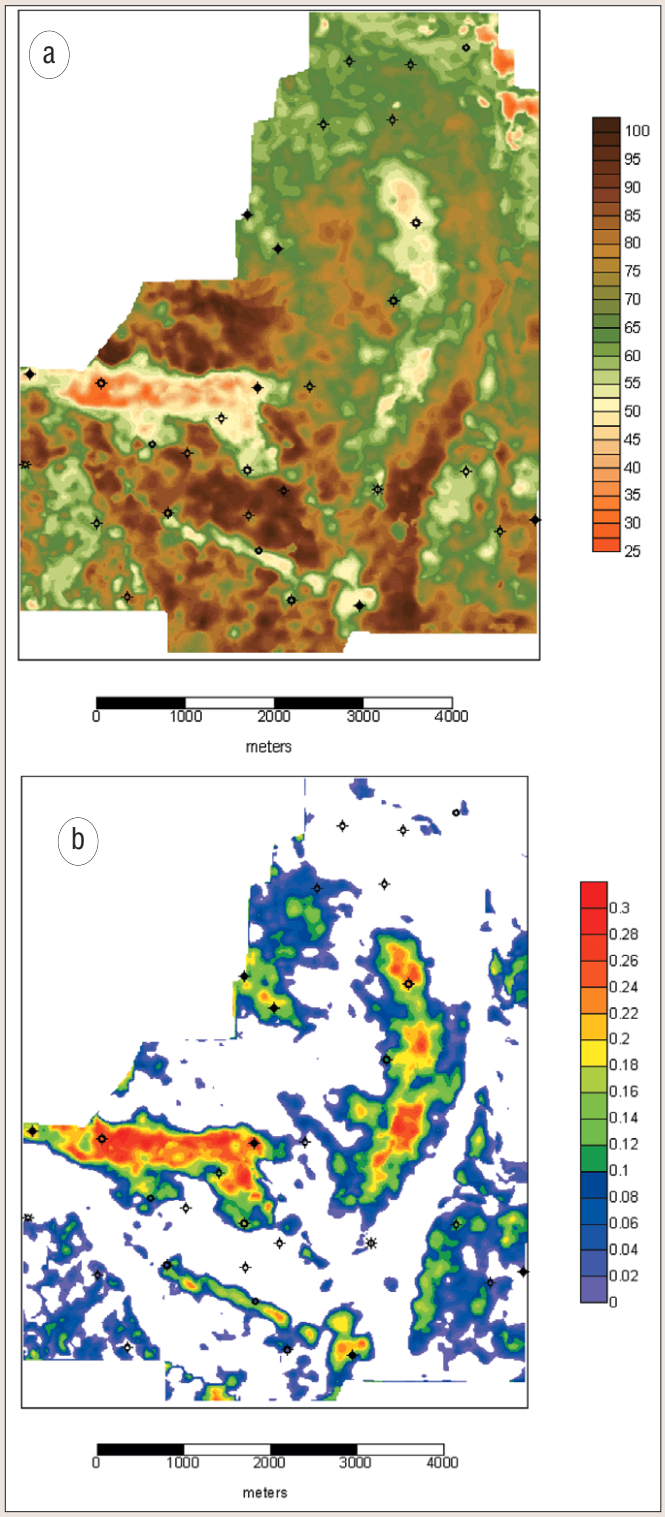

Figure 6. *(a) Neural network inverted gamma-ray response. The horizon slice is the same as referenced in Figure 1. Note the distinct separation of sand from silt and shale not imaged in Figure 1. (b) Neural network computed porosity from inverted density response. The horizon slice is the same as referenced in Figure 1. Note the distinct separation of sand from silt and shale not imaged in Figure 1. The density values have been masked out for gamma ray values representative of silt or shale, giving a relative porosity indicator for the sands.*

where ρ_b = bulk density, ϕ = porosity, ρ_{ma} = a clean formation of known matrix density, and ρ_f = a fluid of average density.

From log data, the sand filled channels are interpreted as having gamma values less than 50 API gamma units. This cut-

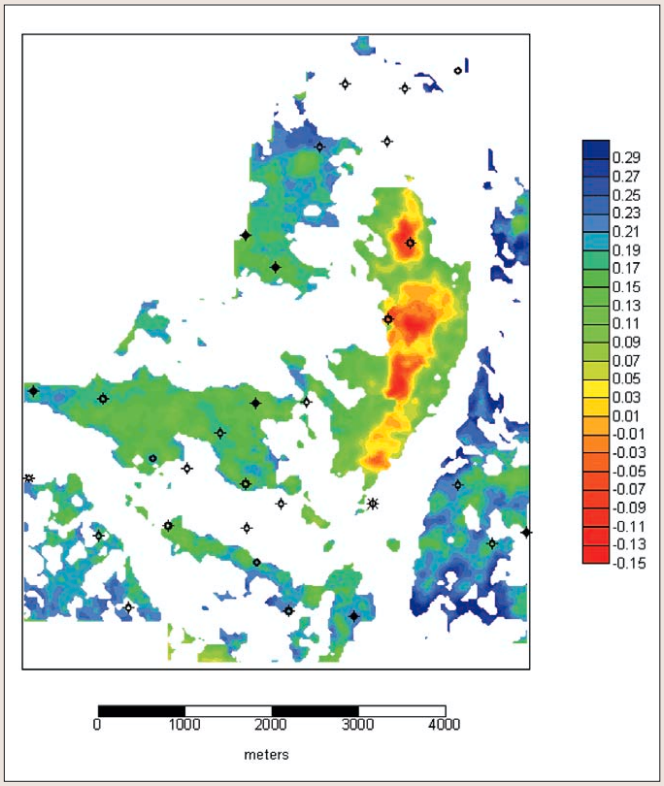

Figure 7. *Computed Lambda representing relative fluid incompressibility. High values of incompressibility such as brine are blue; low incompressibility, red, suggests gas.*

off value was used to mask out inverted density values for silts and shales. Analysis of Figures 6a and 6b shows three distinct sand-bearing channels. The coherence time slice indicates the boundaries of the channels clearly and the gamma ray inversion helps in interpreting major sand bodies within the channels.

The incompressibility coefficient λ (Lambda) was determined by dividing the Lambda Rho value by the inverted bulk density. The results are represented in Figure 7. High values of incompressibility are thought to represent brine and are colored blue. Lower (more compressible) values, green, suggest oil and red suggest gas.

Analysis of the rigidity coefficient μ (Mu) suggests that the sands observed within the longer, north-south trending sand body on the eastern half of the survey contain a different rock type than the sand bodies in the western half of the survey. These results are consistent with the observed production from the two gas wells that penetrate the north-south channel. The geomorphology of this north-south channel indicates that it was deposited during a different depositional cycle than were the other channels, providing an opportunity for a different lithology to be deposited.

Conclusions. AVO inversion results for the estimation of Lamé parameters were successfully integrated with seismic attribute volumes derived from neural network analysis. The results were converted to volumes of log gamma ray and bulk density. These geologically meaningful parameters contributed to the estimation of relative sand distribution, porosity, and fluid content estimates.

Two new drilling locations derived from this work encountered a new gas-charged reservoir, extending the life of the gas pool and adding new reserves to the operating company's portfolio.

Suggested reading. "Amplitude versus offset and seismic rock property analysis: A primer" by Burianyk (*CSEG Recorder*, 2000). "Rock physics of glauconite and glauconitic sandstone reservoirs" by Diaz et al. (*AAPG Bulletin*, 2001). "Integrated geological and geophysical interpretation case study, and Lamé rock parameter extractions using AVO analysis of the Blackfoot 3C-3D seismic data, southern Alberta, Canada" by Dufour et al. (GEOPHYSICS, 2002). "Detection of gas in sandstone reservoirs using AVO analysis: A 3D seismic case history using Geostack technique" by Fatti et al. (GEOPHYSICS, 1994). "AVO and Lamé constants for rock parameterization and fluid detection" by Goodway (*CSEG Recorder*, 2001). "Use of multiattribute transforms to predict log properties from seismic data" by Hampson et al. (GEOPHYSICS, 2001). "Comparison of linear regression and a probabilistic neural network to predict porosity from 3D seismic attributes in Lower Brushy Canyon channeled sandstones, southeast New Mexico" by Leiphart and Hart (GEOPHYSICS, 2001). "A robust joint inversion algorithm for rock property estimation" by Ma (*CSEG Recorder*, 2001). "Extracting meaningful geologic parameters using multiple attribute analysis on AVO derived Lamé rock parameter inversions: 3D seismic case study from southern Alberta, Canada" by Pruden (SEG 2002 *Expanded Abstracts*). *Log Interpretation Principles/Applications* (Schlumberger, 1989). TLE

Acknowledgments: We thank Kicking Horse Resources for permission to publish the results of this study. We also thank and acknowledge Wendy Ohlhauser and Rafed Kasim of Core Lab Reservoir Technologies, Calgary for help in processing the 3D survey and AVO analysis respectively. Coherence Cube is a trademark of Core Laboratories.

Corresponding author: schopra@corelab.ca